The K2: Open-source simultaneous triple-color TIRF microscope for live-cell and single-molecule imaging

Christian Niederauer[1], **Marco Seynen**[1], **Jan Zomerdijk**[1], **Marko Kamp**[1], **Kristina A. Ganzinger**[1]✉

[1]AMOLF, Amsterdam, The Netherlands

✉ **For correspondence:** ganzinger@amolf.nl

Present address: AMOLF physics of functional complex matter, Science Park 104, 1098 XG Amsterdam, The Netherlands

Data availability: Design files and data are available at xx.xxxx/zenodo.xxxxxxx. Data analysis code is available at github.com/GanzingerLab. Up-to-date information about the setup is available at a dedicated K2 homepage.

Funding: This publication is part of project number VI.Vidi.203.037 of the Talent Programme which is financed by the Dutch Research Council NWO (K.A. Ganzinger). C. Niederauer and K.A. Ganzinger acknowledge support by the WISE program of NWO.

Competing interests: The author declare no competing interests.

Abstract

Imaging the dynamics and interactions of biomolecules at the single-molecule level in live cells and reconstituted systems has generated unprecedented knowledge about the biomolecular processes underlying many cellular functions. To achieve the speed and sensitivity needed to detect and follow individual molecules, these experiments typically require custom-built microscopes or custom modifications of commercial systems. The costs of such single-molecule microscopes, their technical complexity and the lack of open-source documentation on how to build custom setups therefore limit the accessibility of single-molecule imaging techniques. To advance the adaptation of dynamic single-molecule imaging by a wider community, we present the "K2": an open-source, simultaneous triple-color total internal reflection fluorescence (TIRF) microscope specifically designed for live-cell and single-molecule imaging. We explain our design considerations and provide step-by-step building instructions, parts list and full CAD models. The flexible design of this TIRF microscope allows users to customize it to their scientific and financial needs, or to re-use parts of our design to improve the capabilities of their existing setups without necessarily having to build a full copy of the K2 microscope.

Introduction

Commercially available fluorescence microscopes for state-of-the-art single-molecule and super-resolution microscopy are often expensive to acquire and lack the flexibility to incorporate custom features beyond already available add-ons. In recent years, a number of open-source projects originated within the super-resolution fluorescence microscopy community, facilitating the design and construction of custom microscopes from the bottom-up. [1–6]. Additionally, stand-alone solutions for various sub-components of single-molecule microscopes have been published as open source hardware projects (*e.g.* focus stabilization [7–9], laser sources [10–13], objective heaters [14, 15] and beam-shaping devices [11, 16–18]). Our microscope design builds on previous open-source projects and our in-house engineering expertise, to provide a cost-effective and flexible solution for single-molecule fluorescence microscopy.

Here, we present a single-molecule total internal reflection fluorescence (TIRF) microscope that is capable of acquiring dynamic single-molecule data with four-color excitation and simultaneous triple-color detection. The microscope uses a single sCMOS camera and projects the fluorescence emission coming from the sample onto different camera regions for each fluorescence channel. Together with homogeneous illumination from a beamshaping device, this enables simultaneous three-color imaging with large fields of view ($73\,\mu m \times 73\,\mu m$) for each channel. The microscope fur-

Box 1. Potential uses of the setup

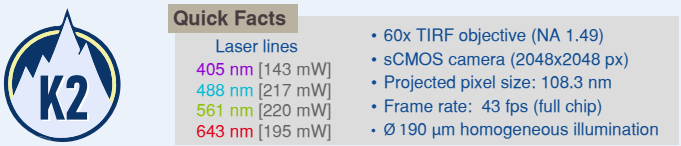

Box 1—figure 1. The K2: Open-source simultaneous triple-color TIRF microscope for live-cell and single-molecule imaging

- (Single-molecule) TIRF microscopy with simultaneous detection of up to three colors
- Experiments with environmental control (temperature) or monitoring (temperature, humidity, sample drift)
- Video-rate recording with camera-triggered excitation (alternating or continuous)
- Timelapse- and multiposition-acquisitions with focus stabilization
- LED-based brightfield imaging
- Widefield epifluorescence imaging
- Fluorescence recovery after photobleaching (FRAP) experiments

Not demonstrated but possible:

- Single-molecule Förster resonance energy transfer (FRET) microscopy
- Multi-color super-resolution microscopy (DNA-PAINT, Photo-activated localization microscopy (PALM), stochastic optical reconstruction microscopy (STORM))

ther features objective heating, a plexiglass cover with an integrated LED array for brightfield illumination, and motorized switching of the angle of the excitation laser beam from TIRF to highly inclined and laminated optical sheet (HILO) and epifluorescence. Finally, the microscope also includes a flip-in lens for fluorescence recovery after photobleaching (FRAP) experiments and a focus stabilization system to correct axial sample drift in timelapse and multi-position measurements.

To ensure reliability and reproducibility of experiments, all imaging settings (*e.g.* laser power, exposure time, stage position, angle of incidence ...) are carefully documented for every dataset. We also monitor and record environmental parameters (temperature, humidity) and the axial sample drift when using the focus stabilization system. This allows us to precisely control and replicate our experiments under identical imaging conditions, which is essential for generating comparable and reproducible data with TIRF microscopes [19].

Setup description

The K2 single-molecule TIRF microscope is comprised of a central cube with the sample stage, sample holder and objective (see ***Figure 1*** and panel I in ***Figure 2***), as well as two enclosed boxes. The box on the right-hand side of the central cube houses the excitation path optics and the focus lock system (see ***Figure 1*** and panel II and III in ***Figure 2***). The box to the left contains the detection pathway, where emitted fluorescence light from the sample is split in up to three spectrally separated channels (see ***Figure 1*** and panel IV in ***Figure 2***). The excitation and detection pathways are enclosed in light-tight aluminum boxes to reduce background light levels, minimize laser safety issues, and prevent dust buildup. The entire setup is mounted on a vibration-damped optical table, with additional components (*e.g.* pre-assembled laser-combiner box, panel V in ***Figure 2***) and the setup control computer located nearby.

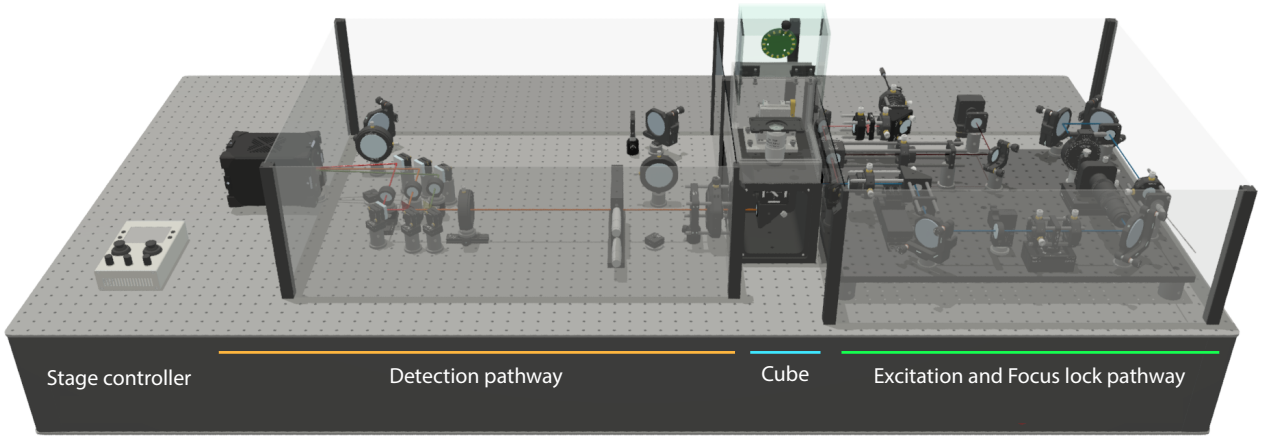

Figure 1. Render of the K2 open-source simultaneous triple-color TIRF microscope for live-cell and single-molecule imaging. For illustration purposes, the two enclosure boxes to the left and right of the central cube are rendered transparent and their lids are removed. The handheld sample stage joystick controller is placed on the optical bench only for illustration purposes and usually located on the computer desk.

Hardware name	K2: Open-source simultaneous triple-color TIRF microscope for live-cell and single-molecule imaging
Subject area	Single-molecule Biophysics, Fluorescence Microscopy
Hardware type	Imaging tool: Total Internal Reflection Fluorescence Microscope
Open source license	CC-BY-NC-ND 4.0
Cost of hardware	137,000 €
Source file repository	xx.xxxx/zenodo.xxxxxxx
Homepage	ganzingerlab.github.io/K2TIRF/K2TIRF/index.html

Microscope body

The K2 single-molecule TIRF microscope is a custom-designed instrument that does not use a conventional microscope body (see ***Figure 3***). The central part is a solid, CNC-milled aluminum block, based on the miCube project [3]. The cube houses the objective, sample stage, dichroic mirror and tube lens. Unlike traditional commercial microscopes, the K2 does not include an objective turret or ocular, as they are not required for our experiments. This design results in a smaller footprint and excellent mechanical stability.

A high numerical aperture oil-immersion objective (NA=1.49, CFI Apochromat TIRF, Nikon) with 60x magnification is mounted on a polyoxymethylene spacer to provide thermal isolation from the cube. A polyimide flexible heater, wrapped around the objective with Kapton foil, and a PT100 temperature sensor glued in place, enable precise temperature control via a proportional-integral-derivative (PID) controller (E5CC, Omron). This design is similar to other custom-made and commercial designs [14, 15, 20], and allows for active heating of the sample, which is thermally coupled to the objective via immersion oil. This enables live-cell imaging and *in vitro* experiments at physiological temperatures.

The sample stage of the K2 single-molecule TIRF microscope is equipped with a three-axis piezo stick-slip positioner (SLS-5252, Smaract) and a two-piece aluminum sample holder that accommodates square ($18\,\mathrm{mm}$ to $26\,\mathrm{mm}$ side length), circular ($25\,\mathrm{mm}$ to $37\,\mathrm{mm}$ diameter) and rectangular ($62\,\mathrm{mm}$ to $80\,\mathrm{mm}$ length, up to $35\,\mathrm{mm}$ width) samples. Samples are held in place with magnets or an aluminum ring to minimize sample drift. The stage is controlled via the computer or a handheld joystick controller (see ***Figure 1***) and accurately positions samples with nanometer resolution

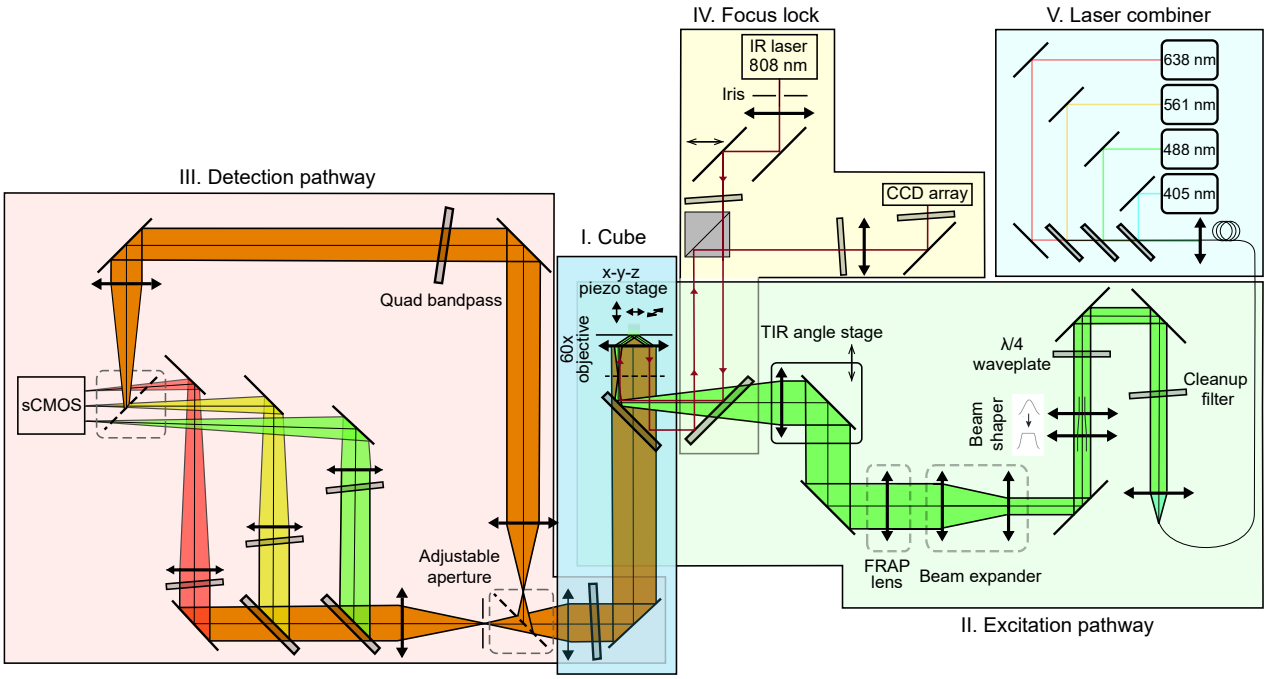

Figure 2. Optical pathway of the K2 microscope: I) The central cube houses the sample stage, objective, dichroic mirror for splitting excitation and emission light, and the tube lens. II) The excitation pathway launches a four-color laser beam with circular polarization and flat-top beam shape into the central cube. The angle of incidence is controlled using a motorized stage to switch between epifluorescence, HILO- and TIRF-imaging. A flip-in lens can be used to focus the beam at the sample plane for bleaching experiments. III) The detection pathway features a triple-color image splitter, projecting the field-of-view onto different regions of the sCMOS camera chip for simultaneous triple-color imaging. Two mirrors on magnetic mounts can be used to bypass the triple-color image splitter. IV) The focus stabilization pathway uses an infrared laser to detect and compensate for axial drift of the sample. V) A pre-assembled laser combiner box delivers the excitation laser beam via a single-mode fiber to the setup.

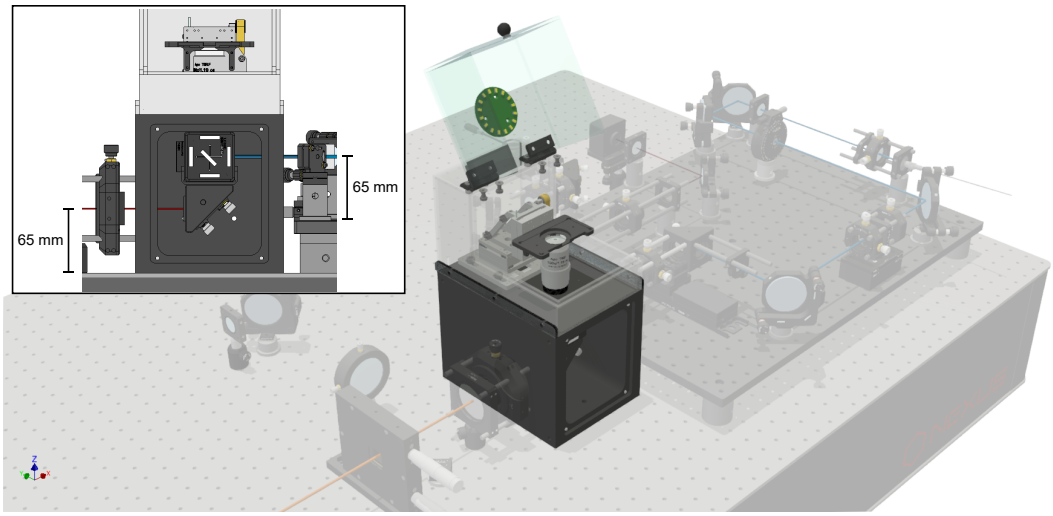

Figure 3. Central cube of the K2 microscope, showing the TIRF objective mounted on a thermal spacer, the sample stage with sample holder, and the dichroic mirror for splitting emitted fluorescence from excitation laser light inside the cube. The plexiglass cover encloses the objective and sample for added thermal stability and protection, and also provides a brightfield light source. Inset: The placement of the detection port on the central cube determines a beam height of $65\,\mathrm{mm}$. The beam height of the excitation path is matched by placing the optical elements on an elevated breadboard, allowing the user to interchange alignment tools and pillar posts between the excitation and detection pathways.

and $30\,\mathrm{mm}$ travel range in all directions, allowing for high-throughput measurements of multi-well coverslides.

The excitation laser beam enters the central cube through a port on the right-hand side and is reflected upwards towards the objective by a dichroic mirror. Residual transmitted laser light is absorbed by a neutral density filter mounted on the dichroic mirror cube. Emitted fluorescence collected by the objective is transmitted through the dichroic mirror and reflected via a mirror towards the exit port on the left-hand side of the cube. A four-bandpass emission filter on the mirror mount blocks remaining laser excitation light from reaching the detection pathway. The dichroic mirror and the right-angle mirror are accessible through a door on the front of the cube, which is held in place with magnets.

The central cube is enclosed by a plexiglass cover that protects the sample and objective from dust buildup and improves temperature stability by minimizing convective air transport. A sensor for temperature and humidity is placed inside the plexiglass box and records the environmental parameters during experiments. The lid of the plexiglass cover includes a LED ring for brightfield imaging of cellular targets. For laser safety considerations, potential adopters of our design may consider using a non-transparent cover.

Excitation pathway

The excitation pathway is mounted on an elevated breadboard, which helps to keep the length of posts short for stability. Custom spacers ($39.7\,\mathrm{mm}$ height) were used to raise the breadboard to the required level, resulting in final beam heights of $65\,\mathrm{mm}$ in both the excitation pathway and the detection pathway. In principle, the beam can be brought up to the required height also by using long enough posts or a periscope-assembly.

We use a commercial pre-assembled laser combiner with a single-mode fiber output for delivering four excitation wavelengths (C-FLEX laser combiner, Hübner Photonics; $405\,\mathrm{nm}$ $140\,\mathrm{mW}$, $488\,\mathrm{nm}$ $200\,\mathrm{mW}$, $561\,\mathrm{nm}$ $220\,\mathrm{mW}$, $638\,\mathrm{nm}$ $195\,\mathrm{mW}$) to the excitation pathway. Laser excitation is controlled by a custom-made laser trigger box, that allows alternating and simultaneous excitation synchronized to the camera exposure. Other approaches to laser triggering include the open-source NicoLase

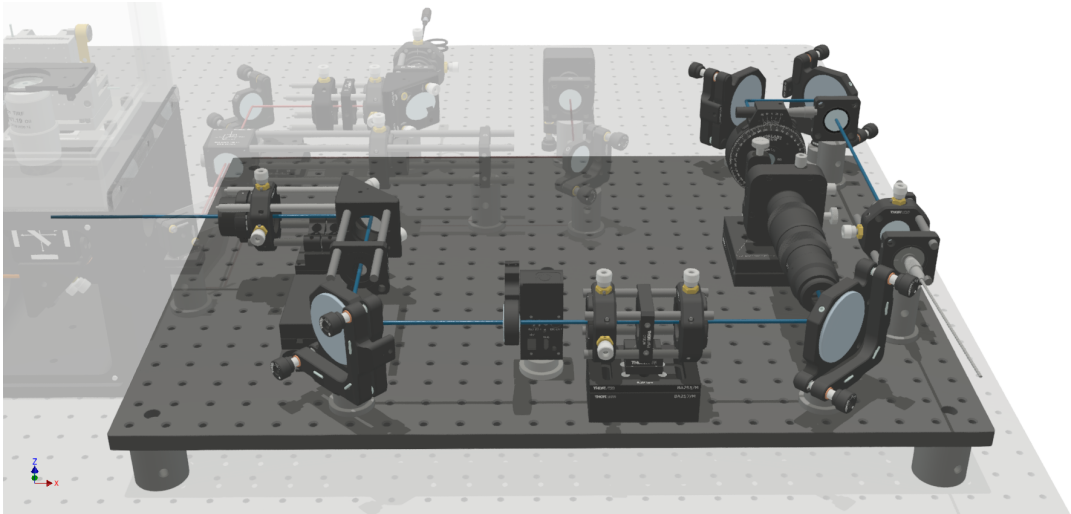

Figure 4. Excitation pathway of the TIRF microscope, featuring (in the order of placement along the optical path) the fiber collimator, laser clean-up filter, quarter-wavelength waveplate, refractive beamshaper, beam expander, flip-in FRAP lens and motorized stage with TIR focusing lens. These components work together to shape and deliver the excitation laser beam to the sample stage, enabling precise control of the angle of incidence for different imaging modes (*i.e.* epifluorescence, HILO, and TIRF). All parts are mounted on an optical breadboard to match the height of the central cube's excitation port.

and SMILE projects [13, 21], as well as the commercial Triggerscope [22].

The TEM00 laser beam is re-collimated after exiting the fiber to a $1/e^2$ beam diameter of $6\,\mathrm{mm}$ (@ $561\,\mathrm{nm}$), directed through a quad-line bandpass for spectral clean-up, and an achromatic quarter-wavelength waveplate to ensure circular polarisation. The Gaussian laser beam profile is transformed into a flat-top profile using a refractive beam shaping device (piShaper 6_6_VIS, AdlOptica, comparable alternative: TopShape TSM25-10-D-B-6, asphericon) [16–18]. A removable telescope magnifies the laser beam by a factor of 2.5, resulting in a beam diameter of $15\,\mathrm{mm}$. The flat-top profile of the laser beam begins to distort as it propagates over longer distances, so we designed the setup to keep the distance between the beam shaper and the objective as short as possible.

For FRAP experiments, an additional lens on a motorized flip-mount can be inserted into the optical path after the telescope, focusing the excitation laser into a $30\,\mu\mathrm{m}$ diameter spot in the imaging plane.

To enable switching between imaging modes (epifluorescence, HILO- and TIRF-imaging, see ***Figure 12***d), the lens focusing the laser beam onto the back focal plane of the objective is mounted on a motorized stage that allows the beam to be translated off-axis while maintaining its parallel alignment with the objective's optical axis.

The lens that focuses the excitation beam onto the back focal plane of the objective is placed as close to the back focal plane as possible, which allows using a lens with a shorter focal length and therefore a bigger illuminated area at the sample plane. Using a telescope with a higher magnification to achieve an equally-sized illuminated area would result in clipping the laser beam, unless larger optics are used throughout the excitation path. To provide more flexibility in the arrangement of the optical elements, future versions of the central cube could be designed with a reduced distance between the objective port and excitation entry port. With the current design, our setup allows for a maximum homogeneously illuminated diameter of $190\,\mu\mathrm{m}$.

Detection pathway

The detection pathway is designed under the assumption that the microscope will mostly be used in a triple-color simultaneous imaging mode. Using a single camera to capture three color channels simultaneously is more cost-effective than using three separate cameras, and combining a 60x

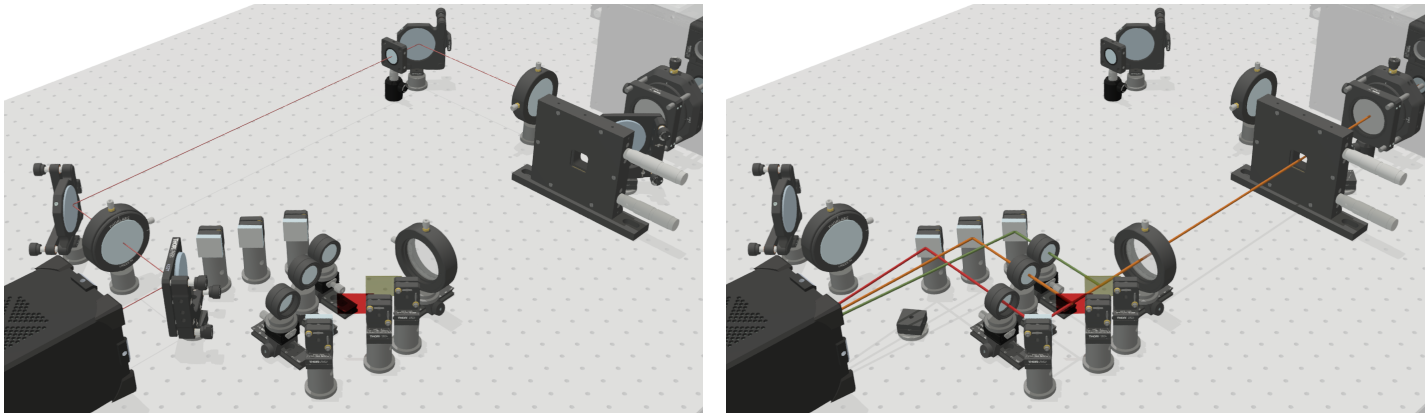

Figure 5. Detection pathway options of the K2 TIRF. Left: single-color full field-of-view path. Right: triple-color detection pathway with adjustable slit aperture and image splitter for simultaneous imaging of up to three color channels.

objective without additional magnification with a 2048x2048 px sCMOS chip allows us to achieve large field-of-views ($73.65\,\mu m$ x $73.65\,\mu m$ per color channel) nevertheless. To achieve even larger field-of-views, the triple-color detection pathway can be bypassed by placing two mirrors on pre-installed magnetic mounts, resulting in a circular field of view of $190\,\mu m$ diameter (see ***Figure 5***). A commercial alternative for image splitting is the OptoSplit (Cairn Research [23]).

As described in the section about the central cube, fluorescence emission from the sample is collected by the objective, passes the quad-bandpass dichroic mirror in the cube and is reflected towards the detection pathway. A quad-line filter blocks residual excitation light from reaching the detection pathway. Emission fluorescence is directed through an infinity-corrected tube lens matching the objective, without further magnification (TTL200-A, Thorlabs). With the camera's physical pixel size of $6.5\,\mu m$, this results in an effective pixel size of $6.5\,\mu m/60 = 108.3\,nm$.

In the triple-color imaging mode, the image of the fluorescent sample is cropped horizontally by a custom razorblade slit aperture in an intermediate image plane. This is necessary to avoid overlapping of the color channels when imaging them side-by-side on the camera chip (see ***Figure S29***). Splitting the fluorescence emission into the different spectral channels and filtering them is done in infinity space in a 4f-configuration. This reduces aberrations and allows more mechanical freedom, since the distance of the second to the first 4f-lens is not critical.

The first 4f-lens is positioned to have its focal plane aligned with the image plane formed by the tube lens. Then, the fluorescence emission is split into three colors by two low-pass dichroic mirrors, matched to the four-bandpass dichroic mirror in the cube, and one dielectric mirror. Furthermore, appropriate bandpass filters are placed in each color channel. Individual lenses mounted on rails and dovetail stages project the images of each color channel next to each other on the camera. The use of individual lenses allows precise co-alignment of the image planes and the correction of residual chromatic aberrations. A dielectric mirror is used in each color channel to project the spectrally-separated images onto the camera chip. Finally, three equally-sized square field-of-views are created by cropping the camera chip horizontally. By cropping in line with the scanning of the sCMOS chip, we are able to reduce the read-out time from $22.6\,ms$ (full chip, 2048x2048) to $7.6\,ms$ (central region, 2048x682). At a typical framerate of 25 fps, this approximately doubles the exposure time per frame ($32.4\,ms/17.1\,ms \approx 1.89$).

The optical path for the image splitter was designed to be as compact as possible to minimize vignetting, while at the same time allowing component accessibility for alignment. Additionally, projecting the image onto the camera at an angle introduces aberrations, therefore the individual focusing lenses and the mirrors are placed as close to each other as possible. As a consequence, this maximizes the distance between the last mirror and the camera and hence decreases the angles at which images are projected from the left and right color channel.

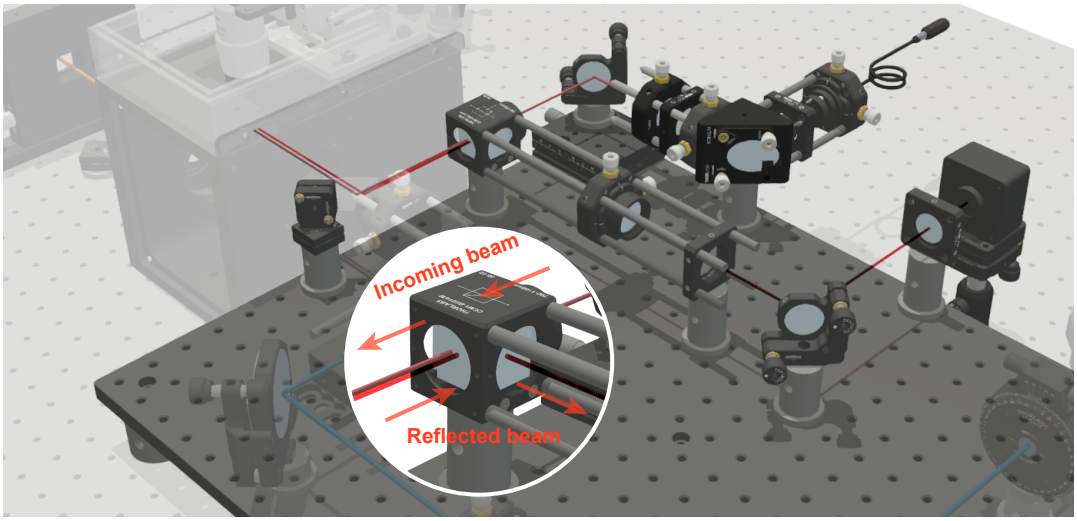

Figure 6. Focus stabilization pathway of the K2 TIRF, mounted alongside the excitation optics on an elevated breadboard. Inset: Separation of incoming infrared laser beam and back-reflected beam by a beamsplitter cube.

In the single-color imaging mode, the full $190\,\mu\mathrm{m}$ diameter illuminated field-of-view is imaged with spatially unseparated color channels. This is accomplished by bypassing the slit aperture and the image splitting pathway using two mirrors, that are placed manually on kinematic magnetic mounts. The first mirror is placed after the tube lens and the second mirror before the camera. Two lenses relay the image in a 4f-system, which conveniently also allows the placement of additional components like filters or phase masks in the fourier plane (see ***Figure 5***a).

Focus stabilization pathway

Axial drift, or movement of the sample along the optical axis, can significantly reduce the sensitivity of TIRF measurements because fluorescence is only emitted from a thin layer. Therefore, keeping the sample in focus is crucial, especially when performing timelapses or (automated) multiposition acquisitions on different areas on a sample. One way to measure and control the distance of the sample from the objective is to use the back-reflection of the excitation laser, with the drawback that measuring and updating the z-position can only be done during the excitation cycle [7]. A dedicated infrared laser is a more versatile option, as it does not excite commonly used fluorescent proteins and dyes, allowing for continuous measurement and control of the sample's axial position without interfering with fluorescence measurements. To use the infrared laser for focus stabilization, the sample is first brought into focus manually and the position of the back-reflected beam is stored. A control circuit then moves the stage to keep the position of the back-reflected beam stable.

Our focus stabilization system, qgFocus (short for **q**uite **g**ood Focus), is similar to other custom-built and commercial focus stabilization designs such as pgFocus [9] or CRISP [8]: A collimated infrared laser is coupled into the excitation path by a short pass dichroic mirror and attenuated with a neutral density filter so that it does not interfere with the fluorescence signals. A manual micrometer stage is used to shift the infrared laser beam off-axis, bringing it into total internal reflection. The infrared laser is then focused at the back focal plane, reflected at the glass-sample interface, and travels back towards a beamsplitter. The back-reflected laser beam is diverted by the beamsplitter towards a bandpass filter and finally focused onto a linescan sensor (TSL1401, Parallax). The intensity curve is registered and fitted with a Gaussian function. A control loop that locks onto the saved in-focus position of the Gaussian function center then moves the piezo-driven sample stage in the axial direction to maintain focus. In our system, manual sample travel in x-y

during focus-controlled experiments is limited to $100\,\mu m\,s^{-1}$ to avoid jumps in the back-reflected beam position that cannot be followed by the control loop.

Scripts

Our microscope control software includes a script interface that allows users to control the setup and perform various tasks using C++ commands. Examples of scripts that can be run using the interface are available at https://github.com/GanzingerLab/K2TIRF/tree/master/K2TIRF/scripts. The available examples include a simple x-y raster scanning script, a laser power calibration method that we used to calibrate the laser percentage settings (see ***Figure S49***) and a script that continuously moves the sample stage up and down, which we used during the alignment process (see ***Figure S26*** and ***Figure SM1***).

Design files

A virtual "copy" of the setup with all optical components has been uploaded to the public repository Zenodo (xx.xxxx/zenodo.xxxxxx). For all custom-made mechanical components, CAD files and technical drawings are provided, following best practices for sharing reproducible microscope hardware [24]. For all custom-made electronic components, PCB layouts and electronic design files are provided. A ready-to-view model is uploaded to Autodesk Drive. The source code of the software for the operation of the setup is uploaded to the Zenodo repository. Python code for processing and analyzing single-molecule imaging data is available at the Ganzinger group Github (https://github.com/GanzingerLab)

Design Files Summary

Description	File type	License	Location of the file
Virtual K2 setup	CAD model	cc-BY-SA-4.0	xx.xxxx/zenodo.xxxxxx
Central cube	Technical drawing	cc-BY-SA-4.0	xx.xxxx/zenodo.xxxxxx
Sample holder	Technical drawing	cc-BY-SA-4.0	xx.xxxx/zenodo.xxxxxx
Thermal spacer	Technical drawing	cc-BY-SA-4.0	xx.xxxx/zenodo.xxxxxx
Plexiglass cover	Technical drawing	cc-BY-SA-4.0	xx.xxxx/zenodo.xxxxxx
Cage assembly adapter plate	Technical drawing	cc-BY-SA-4.0	xx.xxxx/zenodo.xxxxxx
Adjustable slit aperture	Technical drawing	cc-BY-SA-4.0	xx.xxxx/zenodo.xxxxxx
qgFocus unit	Technical drawing, Electronical circuit design, PCB layout	cc-BY-SA-4.0	xx.xxxx/zenodo.xxxxxx
Gustafsson alignment tool	Technical drawing	cc-BY-SA-4.0	xx.xxxx/zenodo.xxxxxx

Bill of materials

The up-to-date bill of materials for the K2 TIRF project is available on the open-access Github page (https://ganzingerlab.github.io/K2TIRF/K2TIRF/component_table.html), providing detailed information on the components and materials needed to build the microscope.

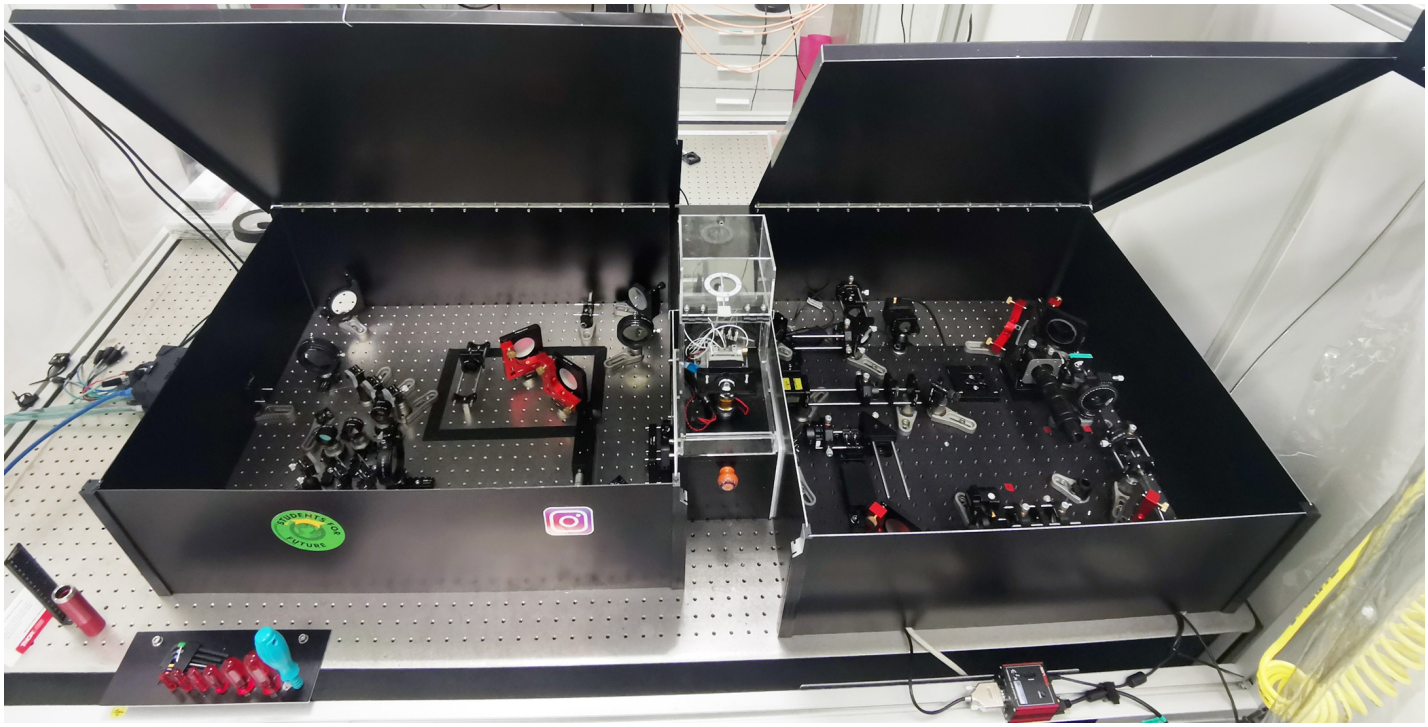

Figure 7. Picture of the K2 TIRF microscope. From right to left, there are the excitation and focus lock pathways on an elevated breadboard, the central cube with the objective, sample stage and a plexiglass cover, and the triple- and single-color detection pathways with the camera on the left. The excitation and detection pathways are enclosed in light-tight aluminium boxes to reduce background light levels, minimize laser safety issues, and to prevent dust from building up.

Build instructions

For an overview of the layout of the optical components, see ***Figure 1*** (CAD-model render), ***Figure 2*** (schematic of the optical pathway) and ***Figure 7*** (picture of the setup). The setup requires approximately $190\,\mathrm{cm}$ by $90\,\mathrm{cm}$ of optical bench space, as well as a similar area (*e.g.* above the optical bench) for the laser combiner, objective heating PID controller and laser trigger box, as well as space for the computer and screens.

When setting up the microscope, the most convenient approach is to start with building and aligning the excitation pathway and use the laser source for alignment. However, if this step needs to be deferred and another laser source is available (*f.i.* the Gustafsson alignment tool), it is possible to begin with the central cube and the detection pathway, since the excitation and detection pathways can largely be assembled and aligned independently of each other. In addition to commonly used alignment tools such as viewing disks, reticles, irises, and calibration slides, we use a cage system mounted on the objective port to simplify the alignment of the excitation path, and the Gustafsson alignment tool for the detection path alignment [25]. The Gustafsson alignment tool is a small diode laser aligned in a mount that is screwed into the objective thread. The wavelength should be situated within one of the fluorescence emission bands, *e.g.* in the GFP-like emission band between $500\,\mathrm{nm}$ and $550\,\mathrm{nm}$. This allows the alignment laser to pass through the emission dichroic mirror, and, if alignment is performed in the correct order, the laser beam can be used to align the entire detection pathway. General approaches and recommendations for the alignment of optical parts are described in [26].

Detailed, step-by-step build instructions are provided in the supplementary information.

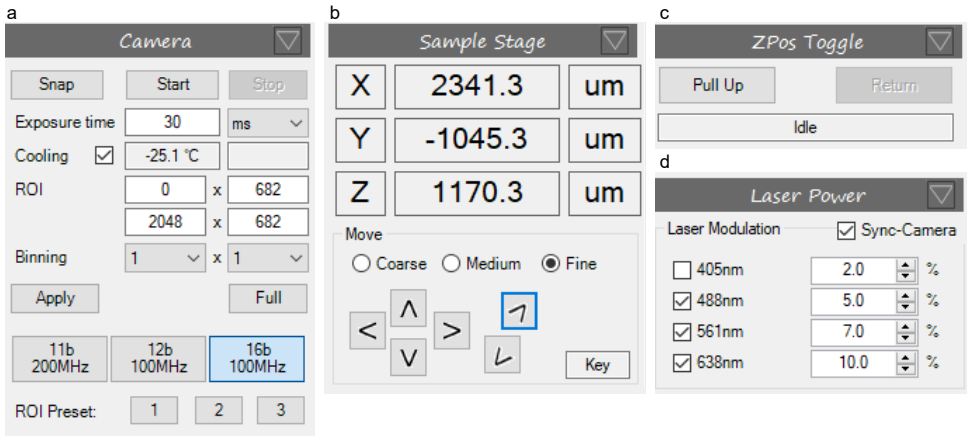

Figure 8. Main control panels of the K2 software: **a**) Camera: In this panel, the exposure time, manual/preset regions of interest (*ROI*), binning and bit-depth of the camera are configured, as well as live-viewing of the camera image (Start/Stop) and snapping a single frame (Snap). **b**) Sample Stage: Piezo stage position readings, and arrow keys (operated via cursor click or with arrow keys on keyboard), complementary to the physical joystick, with three user-defined step sizes. **c**) Zpos Toggle: Toggle for pulling up the sample away from the objective, and returning the sample to the initial z position (*Pull Up*, *Return*). **d**) Laser powers: Laser power settings used during camera live-view, calibrated to achieve a linear percent-to-power relation. The synchronization of the lasers to the camera trigger can be switched off.

Operation instructions

K2 software

A software package for operating the setup was written in C#. It features a graphical user interface (GUI) that provides a simple and intuitive way to control and customize the microscope setup for different experiments. The GUI includes a number of panels for changing settings and directly controlling the various components of the microscope, such as the camera, stage, lasers, and focus lock. ***Figure 8*** and ***Figure 9*** show some of the most important panels for controlling these components. The software also allows users to save experiment routines as templates, with a wide range of custom settings and options.

The source code has been uploaded to the public repository Zenodo (xx.xxxx/zenodo.xxxxxx), excluding any third party software (which we cannot distribute) and excluding internal libraries which are shared among other projects in the institute. Thus, this release will not compile into the final product but it can serve as an inspiration for other development efforts. For all commercial components (sample stage, camera, laser source, flip-in lens, TIR angle stage) LabView virtual instruments, python libraries, and/or plugins for micromanager [27] exist and can be used alternatively for the setup control.

In the following, the operation of the setup is described using the K2 software.

Camera

The camera panel (***Figure 8***a) provides access to all relevant camera settings, such as the exposure time, region of interest, pixel binning, and bit-depth. The Start/Stop buttons can be used to activate or stop the camera live-view streaming (Figure 15), and the Snap button takes a single frame snapshot.

Live-view and RGB viewing mode

The camera image is streamed in the live-view mode, allowing the user to position the sample and to search for a suitable region of interest, as well as to determine appropriate imaging conditions, such as laser power and exposure time. The contrast and colormap settings of the streamed image are set by the user (***Figure S45***). The K2 software also features a RGB viewing mode, that super-

positions the triple-color separated camera channels as a red-green-blue overlay in the live-view (***Figure S46***). This allows to quickly assess colocalization in different channels and therefore speeds up screening for an interesting cell or region of interest on the sample, and is a convenient tool during the alignment of the triple-color image splitter (see ***Figure S26***).

Sample stage

The piezo stick-slip stage is steered both with the software (either by clicking on the sample stage panel arrows, or using arrow keys on the keyboard) and by a handheld joystick controller. To ensure safe and efficient sample handling, the user can adjust the step sizes *Coarse*, *Medium* and *Fine* and define position limits (***Figure S47***).

A z-position toggle is available that improves the experimental workflow and reduces the amount of immersion oil needed for high-throughput measurements. It works by moving the sample upwards away from the objective, with x and y positions unchanged. The sample is first moved slowly (at $0.8\,\mathrm{mm\,s^{-1}}$ for $3\,\mathrm{mm}$), to avoid introducing air bubbles into the immersion oil and to give the fluid time to draw back to the objective (see ***Figure SM2***). The sample can then be exchanged or moved horizontally, and returns to the previous z-position, again approaching the last millimeters towards the objective slowly. This considerably improves the handling when several samples are imaged and need to be exchanged often. When using multi-well samples, or when imaging many different regions on a single sample, the z-position toggle is used for removing the sample from the immersion oil, repositioning in x-y, and moving it back to the original z-position (see ***Figure SM3***). This reduces the amount of immersion oil that has to be reapplied and thus allows for high-throughput measurements with minimal user interaction. The exact values for the distance and speed limits are user-defined in the K2 software backend settings (***Figure S48***).

Laser powers

The laser powers panel controls laser on/off state and excitation power, and features the option to deselect synchronization of the excitation to the camera exposure. A linear relation between the power percentage set by the user and the actually delivered laser power is established in an initial calibration step (see ***Figure S49***).

qgFocus

In the qgFocus panel, the focus lock sensor's exposure time and number of averaging cycles are set (***Figure 9***). Within an axial range of about $5\,\mu\mathrm{m}$ around the samples' in-focus position, the back-reflected infrared laser is registered as a sharp peak on the qgFocus sensor and fit with a Gaussian function. For locking the focus position, the center position of the Gaussian fit is saved and used as the setpoint for a control loop.

Action point: During the initial usage of the setup, determine the control loop variables to ensure that the focus position stabilizes within a few seconds after moving the sample in x-y (used values: proportional gain 0.7, integral time $2\,\mathrm{s}$, integral limit $1 \times 10^{10}\,\mathrm{s}$).

Once the focus lock is engaged, the qgFocus panel displays the extent to which the stage has been shifted to maintain the sample in focus. The sample stage movement is restricted to a speed of $100\,\mu\mathrm{m\,s^{-1}}$ to allow the qgFocus to follow the sample's z-position continuously. This speed limit can be defined by the user in the K2 software backend settings (***Figure S50***).

Angle of incidence

The motorized TIR stage sets the angle of incidence of the excitation laser beam, allowing the user to switch between epifluorescence, HILO and TIRF imaging modes by calling user-defined positions on the Angle of Incidence panel (see ***Figure 9***).

Action point: When operating the setup the first time, the TIR stage positions corresponding to the different imaging modes are determined with a fluorescent sample (*e.g.* dye in solution) mounted: Starting from the epifluorescence position after setup alignment, the TIR stage is initially

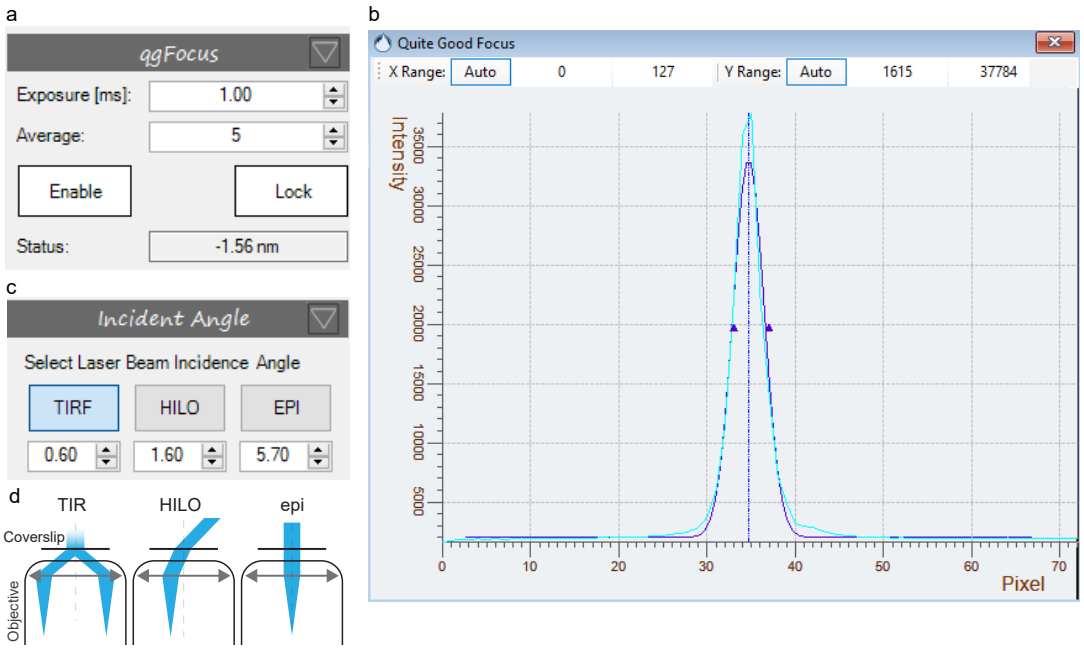

Figure 9. a) qgFocus control panel to switch on the focus lock sensor (*Enable*), to lock onto a focus position (*Lock*) and to set the exposure time and number of averaging cycles. The *Status* reports on the current distance of the stage with respect to its initial z-position. **b**) qgFocus sensor output displaying the measured back-reflected laser intensity profile on qgFocus sensor (cyan line) and a Gaussian fit to the intensity profile (blue line). **c-d**) TIR stage panel: Stage positions for TIRF, HILO and epifluorescence imaging are set and can be called during the experiment to change the angle of incidence of the excitation laser beam.

moved $4.5\,\mathrm{mm}$, and then in steps of $0.1\,\mathrm{mm}$. The transition from epifluorescence to TIRF imaging is easy to recognize (see [28] for a detailed description), as interference patterns caused by specs of dust scattering the coherent excitation laser beam, become visible. In sparse single-molecule type of samples, these interference patterns are not visible, but the transition is marked by a sharp increase in the signal-to-background ratio [4]. HILO imaging, where the laser beam penetrates the sample at an angle instead of being totally internally reflected, is typically performed close to the TIR setting (*i.e.* between $4\,\mathrm{mm}$ to $5\,\mathrm{mm}$ from the epifluorescence position).

Pre-configuring experiments

Imaging conditions and sequences may be pre-configured as saveable experiment configuration file (**.k2m*) and can be reused as templates. The user can choose from three general modes: a) Sequence acquisitions, where a pre-programmed laser excitation sequence is looped through every timepoint - for a user-defined number of times, allowing for both alternating laser excitation style experiments and simple timelapses. b) Video acquisitions at the maximum camera framerate, with one or several lasers simultaneously activated. c) z-stacks, where images are taken at pre-defined axial positions, with one or several lasers switched on.

Each of these modes can be combined with a FRAP experiment at the beginning of the recording, or a multiposition acquisition. During a multiposition acquisition, the software performs the pre-configured acquisition at different, pre-defined stage positions.

The experiment configuration, sample name and optional comments are saved as a **.txt* file along with the microscopy data (**.raw* and **.yaml*.)

Sequence acquisition

For certain experiments (*e.g.* FRET), fluorophores need to be (alternatingly) excited by a single excitation wavelength at a time. This can be done by performing a Sequence Acquisition. Any excitation

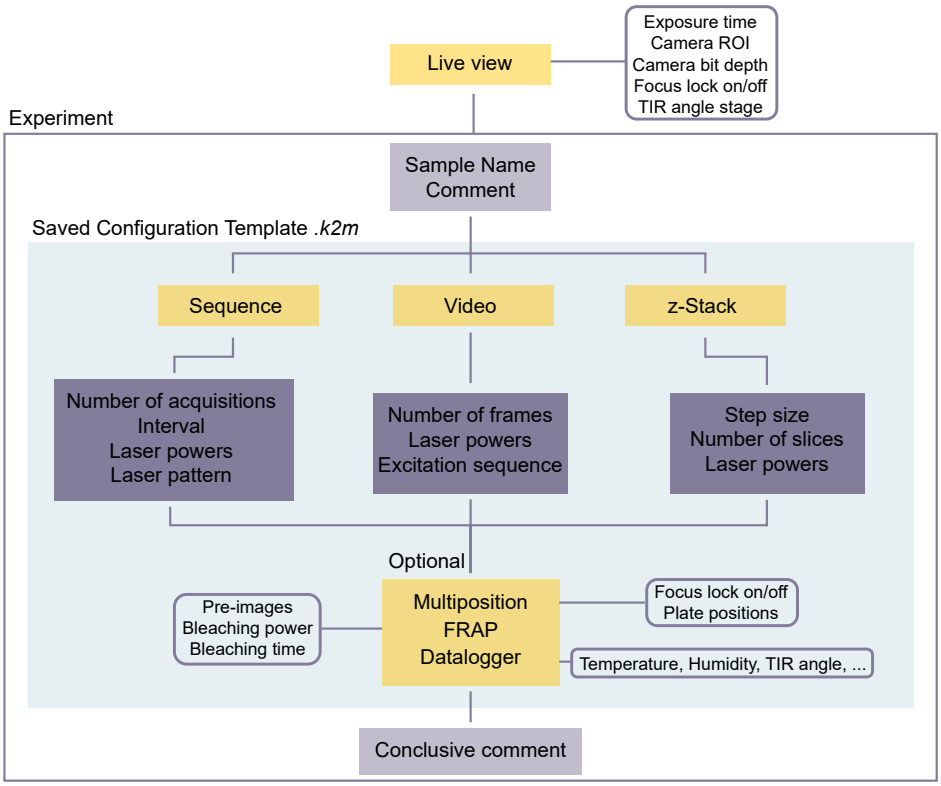

Figure 10. Experiments configuration diagram: Experimental settings are optimized during live-view. An acquisition is then performed by configuring, or reusing a experiment configuration template and adding details about the sample and experimental conditions. For the acquisition itself, three options (*Sequence*, *Video* and *z-Stack*) are available and for each option, the necessary settings are configured. Optionally, the experiment can be performed at different sample positions (*Multiposition*), as a *FRAP* experiment, and with additional recording of environmental parameters. After the experiment is performed, a comment may be added to the file.

sequence, with one or several lasers excited during a given camera frame, can be pre-programmed, and is looped through for every timepoint throughout the duration of the experiment. The interval between each timepoint can be set, which also allows for timelapse recordings.

Video acquisition

The video acquisition mode allows the simultaneous imaging of multiple color channels, *e.g.* for multi-color single-molecule tracking experiments, at the maximum camera framerate without intervals between acquired frames. For every frame, the same pre-defined set of lasers at a certain power percentage will be used to excite the sample. Additionally, there is the option to use in-frame alternating laser excitation. For simultaneous imaging of blue excitable dyes (*e.g.* ATTO488) and cyanine dyes (*e.g.* ATTO643), this was demonstrated to decrease the bleaching of red dyes induced by the $488\,\mathrm{nm}$ laser drastically [29]. The duration of the pulses is set to be at least ten times smaller than the total frame exposure time, and the triggering scheme is such that the $488\,\mathrm{nm}$ laser is pulsing anti-cyclic with respect to the others (see ***Figure S51***).

zStack

Although TIRF microscopy implies collecting fluorescence from the sample surface plane, most TIRF setups allow changing the angle of incidence to HILO or epifluorescence imaging. In these imaging modes, a z-stack can deliver additional information along the axial dimension. The K2 software requires a starting z-position, the number of slices and z-step per slice and will record one frame per slice with a given laser power and exposure time. During the acquisition, the focus lock is disengaged and the sample is moved back to the original z-position after the last slice.

FRAP

Fluorescence recovery after photobleaching (FRAP) is a method for studying diffusion dynamics by bleaching the sample locally and observing the recovery of fluorescence by diffusive exchange of unbleached fluorophores into the bleached area. A FRAP experiment in the K2 setup is performed by collecting a number of pre-bleaching frames (either in Sequence- or Video-mode), followed by a bleaching phase where the flip-in lens is flipped into the excitation path, the power of one or several lasers is increased. After the bleaching phase, the recovery is recorded using the Sequence- or Video-mode (see ***Figure SM4***). Between bleaching and the recovery phase, a short delay is introduced to account for the finite flipping time of the flip-in lens (flip-in: $0.5\,\mathrm{s}$, flip-out: $1\,\mathrm{s}$). The area and the position of the bleached spot is determined by the positioning and focal length of the flip-in lens.

Multiposition acquisition

Coordinates (x, y and z) of stage positions can be generated (*e.g.* for a raster scanning of the sample, see ***Figure S52***), saved in a list and called manually, or automated during an experiment where a pre-designed (sequence, video, and/or FRAP) acquisition is performed at each position of the coordinate list (see ***Figure SM3***). If the focus lock is engaged, the stored z-position is ignored.

Starting up the setup

Before turning on the lasers, verify that any removable optical component (beamshaper, beam expander, mirrors for bypassing the triple-color pathway) and filters are placed correctly depending on the experimental requirements. Make sure that the flip-in lens is flipped out, the TIR stage is in a safe position, the objective correction collar is in the correct position, and that the objective was cleaned properly by the last user. If heating is required, make sure to turn it on about $30\,\mathrm{min}$ before the experiment, to allow the temperature to stabilize (see ***Figure 14***).

Switch on the required power supplies (lasers, camera, camera cooling, motorized stages and mounts, computer) and mount the sample. Open the setup control software and initialize the motorized stages. Switch on the appropriate lasers at a low power and start the qgFocus and the

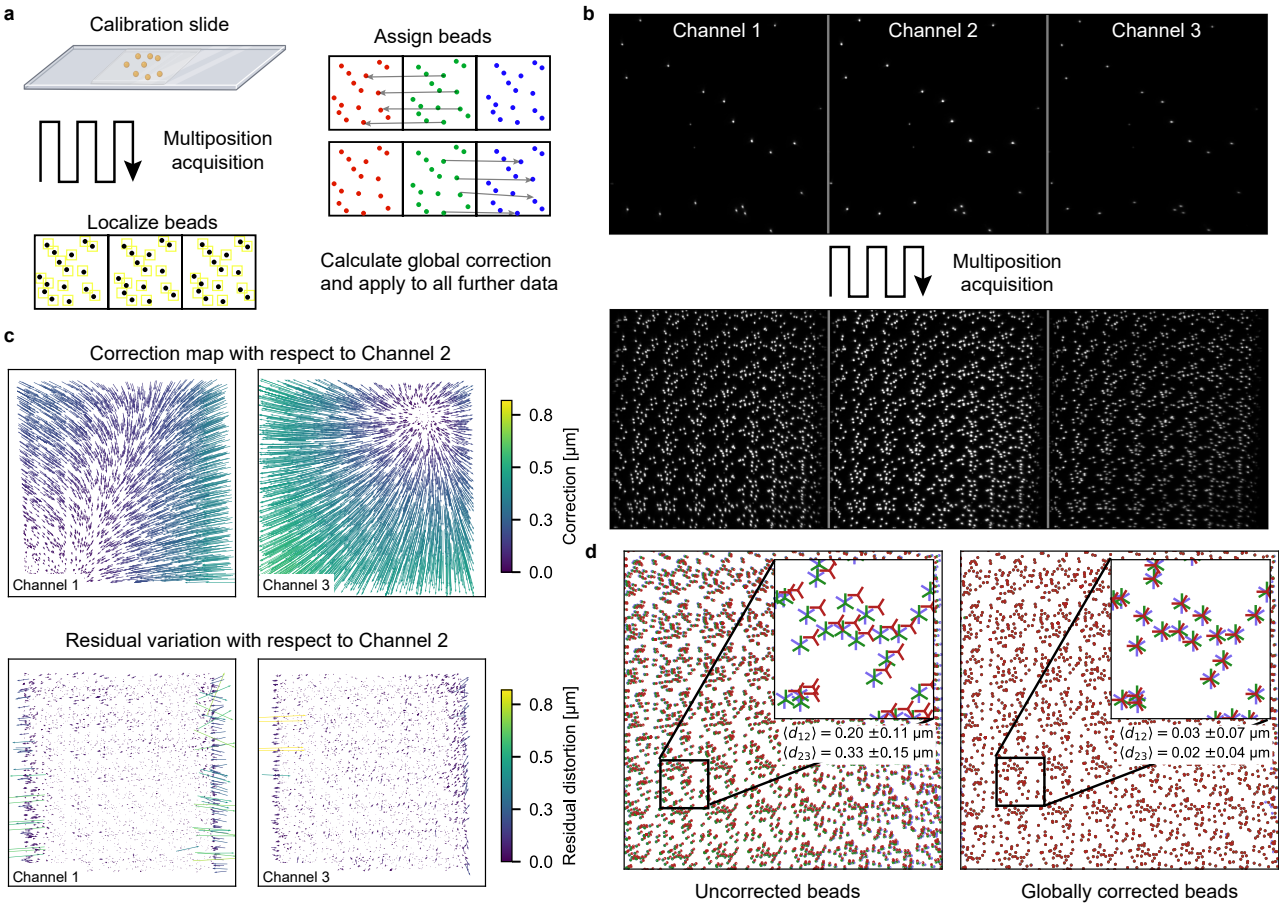

Figure 11. Multicolor channel alignment
a) Multicolor-labeled Tetraspeck beads are deposited sparsely on a coverslide and imaged at multiple positions to collect a large number of $x-y$ sample points. Identical beads are identified in the three color channels and localized frame-by-frame. Variations of bead $x-y$ coordinates relative to the center channel are calculated pairwise, and used to compute a global correction map. This correction map is then used to correct single-molecule localizations acquired in further experiments. **b)** Upper row: Image of Tetraspeck beads in the three color channels, for a given sample position. Lower row: Maximum projection of all bead images acquired during a multiposition raster-scan. **c)** Upper row: Correction maps of left and right channel, with respect to the middle channel. Lower row: Residual spatial variation remaining after the correction is applied to the calibration data. Arrows indicate the direction of the necessary correction, with their length and color representing the amount of correction needed. **d)** Superimposed $x-y$ positions of Tetraspeck beads with uncorrected coordinates (left) and corrected coordinates (right), with average spatial variations $\langle d_{12}\rangle$ and $\langle d_{23}\rangle$ of identical beads in the left and right channel, with respect to the middle channel.

live-view of the camera. Bring the sample into focus using the sample stage joystick controller. As described before, during the initial operation, the qgFocus control loop settings and the TIR stage positions for epifluorescence, HILO and TIRF imaging should be determined to ensure optimal imaging performance.

Validation and characterization

Multicolor channel alignment

Chromatic dispersion and misalignment of optical elements in the detection pathway lead to distortions across the different color channels, complicating the analysis and interpretation of multicolor microscopy data. Especially for (single-molecule) colocalization experiments, different color channels need to be precisely co-aligned. The physical alignment of the color-splitting optical path is done while imaging a calibration slide and superimposing the three color channels, as described in the supplementary build instructions (see ***Figure S26***). In doing so, we achieve an average spatial variation across different color channels below $1\,\mu\mathrm{m}$. The remaining spatial offset between the

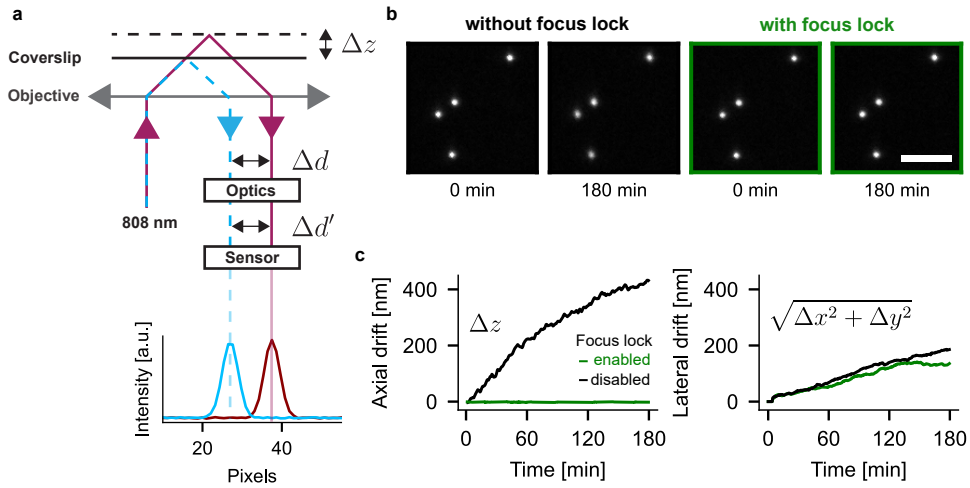

Figure 12. a) Schematic of the qgFocus lock: an infrared laser beam is focused off-center at the back focal plane of the objective and is totally internally reflected at a coverslip. Upon an axial movement Δz of the coverslip, the reflection of the beam is shifted laterally by a distance Δd, which is translated into a distance $\Delta d'$ through downstream optics. A sensor registers the intensity profile of the back reflected beam and determines its center by a Gaussian fit. A control loop acting on the sample stage moves the sample such that the displacement of the currently measured intensity profile and of the referenced intensity profile is approaching zero. **b**) Still frames of a sample of fluorescent beads, imaged with and without qgFocus. For the experiment without focus lock, there is a blurring of beads observable over time, whereas the beads with the focus lock enabled stay in focus throughout the entire experiment ($180\,\mathrm{min}$). For both experiments, the same sample was used, but before each acquisition, the sample was withdrawn from the immersion oil and re-positioned, to avoid biases due to non-identical settling times of the mounted sample. One frame was captured every $30\,\mathrm{s}$ for three hours. Scale bar is $5\,\mu\mathrm{m}$. **c)** Representative axial and lateral sample drift during a three hour experiment with and without enabled focus lock. Left: Axial drift , Right: Lateral drift of tracked beads, as given by the euclidean distance of their current position versus their position in the first frame.

channels is then corrected computationally: first, accumulated bead positions from raster scanning the calibration slide are assigned throughout the corresponding channels (see ***Figure 11***a-b). A spatial correction map is then calculated (***Figure 11***c) using a recently introduced method based on Zernike polynomial gradients [30]. Using this correction map, mean residual spatial variations are below $30\,\mathrm{nm}$ (***Figure 11***c-d).

Sample drift and focus stabilization

For timelapse measurements, multi-position acquisitions and super-resolution experiments, sample drift can significantly degrade the quality of the recorded data [31]. In single-molecule or live-cell experiments, lateral drift of the sample usually does not interfere with the experiments as the typical drifting appears on much slower timescales than the molecular movement that is being studied (lateral sample drift in our setup: $\approx 1\,\mathrm{nm\,min^{-1}}$, diffusion of individual receptor proteins in cell membranes: $\approx 0.1\,\mu\mathrm{m^2\,s^{-1}}$ to $1\,\mu\mathrm{m^2\,s^{-1}}$). Axial sample drift, however, leads to a shift of the focal plane. For samples with significant three-dimensional expansion, this can result in a shift of the observation plane, leading to a decreased signal-to-background ratio due to the defocus blurring of the point spread function, or even the loss of the object that the user initially focused on. Specifically in TIRF microscopy, in which fluorescence is emitted only from a thin layer close to the coverslip, the axial sample drift should be minimized to ensure optimal signal-to-background ratios.

To mechanically correct axial drift, we use an active control mechanism that reacts to the lateral displacement Δd of a totally internally reflected infrared laser beam, caused by an axial shift Δz of the sample (***Figure 12***a). The back-reflected laser beam is then relayed through additional optics, resulting in a displacement $\Delta d'$, that is determined by comparing the center peaks of the reference

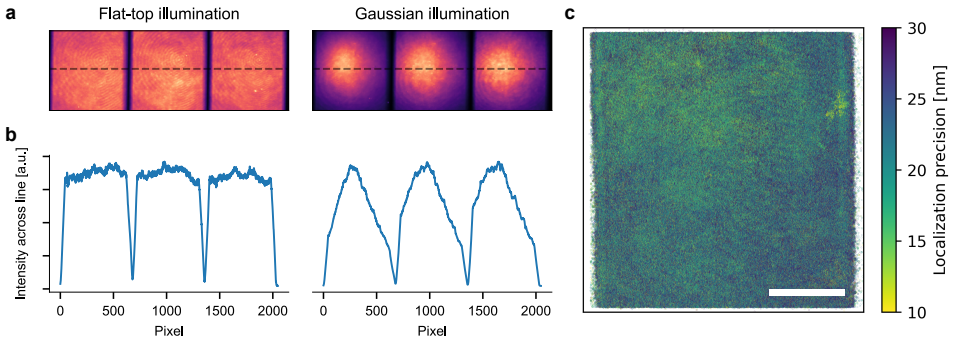

Figure 13. Triple-color TIRF imaging of a multicolor fluorescently labeled bilayer, excited by a spatially homogeneous excitation field (**a**) versus a Gaussian beam (**b**). Laser intensities were adjusted for each color channel to produce similar peak intensities. Fields of view per color channel are 682x682 pixels, or $73.656\,\mu m$ x $73.656\,\mu m$. **c)** Localization precision map computed from a total of 3,300,599 individual localizations of freely diffusing Cy3B-labeled reconstituted proteins on a supported lipid bilayer. The homogeneous excitation field allows precise localization of single-molecules across the entire field-of-view. Scale bar: $20\,\mu m$.

and the currently measured laser profiles on a line-array sensor.

We evaluated the axial and lateral drift of our K2 TIRF microscope with and without enabled focus lock during a three hour experiment. Fluorescent beads (TetraSpeck Microspheres, $0.2\,\mu m$) mounted on the surface of a microscope slide were used as fiducials. The axial drift during experiments without focus lock (***Figure 12***b) is observable as a slight blurring of the beads, which is not the case for experiments with enabled focus lock. The axial sample drift was quantified by converting the lateral displacement of the back-reflected laser on the sensor into an axial distance. The displacement-to-pixel was determined in an initial calibration experiment (***Figure S50***, $1\,px \triangleq 561\,nm$). ***Figure 12***c shows the axial drift throughout the three hour experiment exceeded $400\,nm$ without focus lock, whereas virtually no residual drift was detectable when the focus lock was enabled ($< 10\,nm$). Lateral drift was quantified by tracking the fiducial beads and calculating their euclidean distance from their original position at the start of the experiment. We found the lateral drift to be similar with and without focus lock enabled, which is expected since the focus lock only compensates the axial drift. In comparison to other setups [32–34], the lateral drift is extremely low ($\approx 200\,nm$ in three hours), which is likely due to using a closed-loop piezo stage not only for the z-axis, but also for x- and y-axes. Most commercial and home-built setups use servomotors for the x- and y-axes, with at least one order of magnitude worse resolution and stability [32, 35, 36].

Large field-of-view and illumination homogeneity

One of the key features of the K2 TIRF microscope is its large field-of-view that is flat and homogeneously illuminated, which facilitates conducting statistically sound and quantitative single-molecule fluorescence experiments. Using a refractive beamshaper and appropriate optics, we are able to evenly illuminate a large field of view up to $190\,\mu m$ in diameter, providing a high signal-to-background ratio across the entire field of view. This is especially important for dynamic live-cell or single-molecule tracking experiments (*e.g.* cellular activation essays, kinetic studies of molecular interactions), because events may be non-recurrent and capturing as much data from a single field of view as possible with little to no spatial variation in imaging quality is essential (***Figure 13***c).

In addition, the large 2048x2048 px camera chip allows the imaging up to three color channels simultaneously side-by-side without the need to invest in multiple, synchronized cameras. Simultaneous capture of multi-color emission is important for accurately tracking fast dynamic processes of multiple species of fluorescently labeled molecules in cellular and artificial environments. For triple-color simultaneous imaging, the camera is cropped to produce three equal-sized fields of view of 682x682 pixels, or $73.656\,\mu m$ x $73.656\,\mu m$ (see ***Figure 13***).

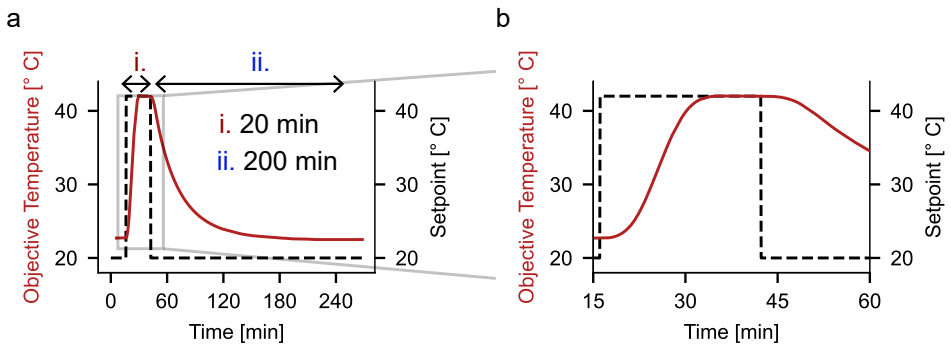

Figure 14. a) Heating phase, stabilized temperature and cooling phase during an objective heating cycle with a setpoint temperature of $42°$, corresponding to $37°$ sample temperature. **b)** Close-up showing stabilized temperature about $20\,\mathrm{min}$ after activating the objective heating.

Furthermore, the homogeneous illumination of the field of view of the K2 microscope not only provides a high signal-to-background ratio across the entire field of view, but also enables seamless stitching of images acquired by raster-scanning the sample. This is because the lack of vignetting at the edges of the field of view allows the individual images to be easily combined into a single, large image without loss of quality (see ***Figure S54***). Furthermore, the focus stabilization system is able to compensate for coverslip tilt and inhomogeneities that can degrade the image quality during raster-scanning. This allows us to perform fully automated raster-scanned image acquisitions, without the need for manual intervention to maintain focus (see ***Figure SM3***).

Objective heating stability and response time

We use an objective heater to maintain a stable, physiological temperature of the sample during extended live-cell imaging at $37\,°\mathrm{C}$. The heater is controlled by a feedback loop that uses a temperature sensor at the objective to control the flow of current through a polyimide heater wrapped around the objective. Thermal decoupling of the objective and a plexiglass enclosure around the central cube help to maintain a constant temperature. The offset of objective temperature and the temperature directly at the sample was determined using a second sensor immersed in a test sample. At a room temperature of around $21\,°\mathrm{C}$, the system stabilizes at an objective temperature of $42\,°\mathrm{C}$ (corresponding to $37\,°\mathrm{C}$ at the sample) after about $20\,\mathrm{min}$ (***Figure 14***). Since there is no active cooling, it takes about $200\,\mathrm{min}$ for the system to return to room temperature. The thermal isolation and the mass of the central cube ensure minimal heating of the rest of the setup, which is important for maintaining alignment. In fact, the environmental sensor on the central cube showed an increase in temperature of less than $1\,°\mathrm{C}$ when the objective was heated to $42\,°\mathrm{C}$ (***Figure S53***). Overall, the objective heater is an effective and low-cost solution for maintaining a stable, physiological temperature of the sample during live-cell imaging.

Experimental applications: from live-cell imaging to single-molecule tracking

The K2 TIRF microscope can be used for a wide range of live-cell and single-molecule experiments. ***Figure 15*** showcases several such applications: dual-color single-molecule tracking of membrane proteins on live cells, with the third channel being used for detecting a transfection reporter (1) and dual-color single-molecule tracking of reconstituted membrane proteins transiently forming dimers on a supported lipid bilayer (2), as well as timelapse imaging of immune cell activation (3). Epifluorescence imaging of giant unilamellar vesicles is shown in (4), alongside brightfield imaging of an immune cell using the circular LED array. Combining epifluorescence imaging together with the z-stack function allows to capture 3D volumes of cells in suspension (5). The K2 TIRF microscope is also capable of performing fluorescence recovery after photobleaching (FRAP) experiments, here shown on a COS7 cell labeled with a fluorescent membrane marker (6).

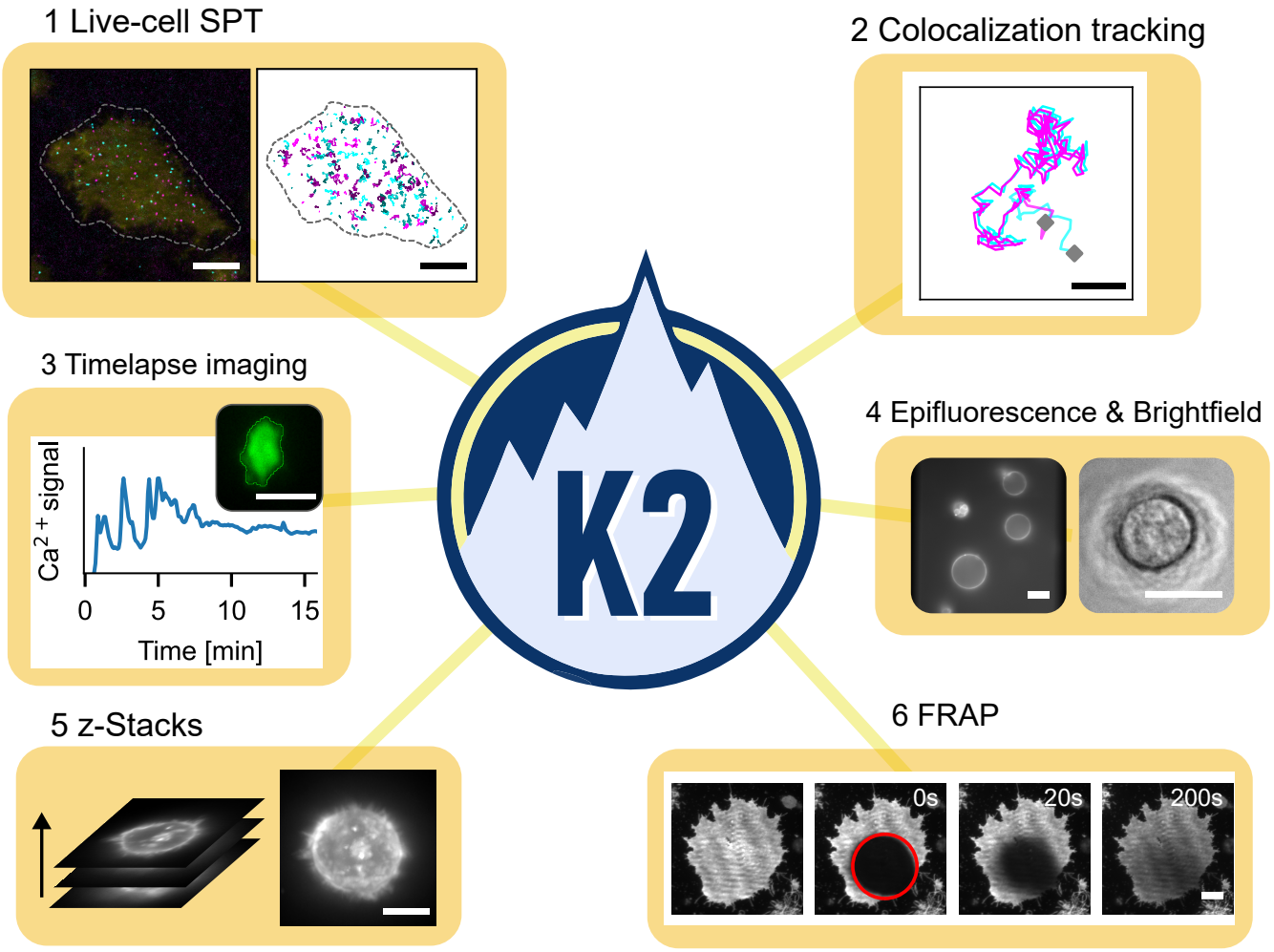

Figure 15. Examples of the experiments that can be performed with the K2: (1) Dual-color single particle tracking on live Jurkat T-cells with a third channel used as a transfection reporter and (2) dual-color single-molecule tracking of reconstituted proteins on a supported lipid bilayer. Tracking the movement of two (or more) different fluorescently labeled molecules provides information about the interactions between different molecules by colocalization analysis; (3) Live-cell timelapse imaging to measure immune cell activation: Jurkat T-cell outlines are tracked using cellpose [37] and TrackMate [38] and the mean intensity of the cell-permeable green fluorescent Ca^{2+} reporter Fluo4 is measured. (4) Epifluorescence imaging of giant unilamellar vesicles (left) and brightfield imaging of an adherent Jurkat T-cell (right). (5) Maximum projection of a z-stack of a Jurkat T-cell in suspension, imaged in epifluorescence mode. (6) Timeseries of a fluorescence recovery after photobleaching measurements on a COS7 fibroblast cell: A reference image before the photobleaching step (left), directly after a bleaching pulse in the red circle ($0\,\mathrm{s}$, and the subsequent recovery after $20\,\mathrm{s}$ and $200\,\mathrm{s}$, showing the mobility of the fluorescently labeled membrane. All scale bars: $10\,\mu\mathrm{m}$

In summary, the K2 TIRF microscope is a versatile instrument that allows the study of cellular and molecular dynamics in up to three fluorescence channels with an additional brightfield option. A large and homogeneously illuminated field-of-view and the highly-automated sample positioning and raster-scanning options enable the acquisition of high-quality microscopy data with comparatively high throughput and little demand on user input. Furthermore, imaging experiments can be performed for extended durations (hours) due to the setup's excellent stability, active focus stabilization and objective heating for live-cell compatibility. The extensive open-source documentation should allow researchers to easily recreate the setup, or parts of it, and adapt it to their specific requirements.

Acknowledgment

This preprint was created using the LaPreprint template (https://github.com/roaldarbol/lapreprint) by Mikkel Roald-Arbøl. We would like to thank Chi Nguyen for providing timelapse movies of Jurkat T-cell activation acquired on the K2 TIRF setup. We acknowledge support from AMOLF mechanical, software and electronical engineering departments, as well as from the precision manufacturing department. In particular, we would like to thank Marco Konijnenburg, Dico Kruining, Bob Krijger, Henk-Jan Boluijt, Hinco Schoenmaker, Niels Winkelaar and Jan van der Linden for their various contributions. We thank Dr. Philipp Blumhardt for expert advice on TIRF setup construction.

References

[1] Hongqiang Ma et al. "A Simple and Cost-Effective Setup for Super-Resolution Localization Microscopy". In: *Sci Rep* 7.1 (2017), p. 1542. ISSN: 2045-2322. DOI: 10.1038/s41598-017-01606-6.

[2] Alexander Auer et al. "Nanometer-Scale Multiplexed Super-Resolution Imaging with an Economic 3D-DNA-PAINT Microscope". In: *ChemPhysChem* 19.22 (2018), pp. 3024–3034. ISSN: 1439-7641. DOI: 10.1002/cphc.201800630.

[3] Koen J. A. Martens et al. "Visualisation of dCas9 Target Search in Vivo Using an Open-Microscopy Framework". In: *Nat Commun* 10.1 (2019), p. 3552. ISSN: 2041-1723. DOI: 10.1038/s41467-019-11514-0.

[4] Mohammad Nour Alsamsam et al. "The miEye: Bench-top Super-Resolution Microscope with Cost-Effective Equipment". In: *HardwareX* 12 (2022), e00368. ISSN: 2468-0672. DOI: 10.1016/j.ohx.2022.e00368.

[5] John S. H. Danial et al. "Constructing a Cost-Efficient, High-Throughput and High-Quality Single-Molecule Localization Microscope for Super-Resolution Imaging". In: *Nat Protoc* (2022). ISSN: 1754-2189, 1750-2799. DOI: 10.1038/s41596-022-00730-6.

[6] Johannes Hohlbein et al. "Open Microscopy in the Life Sciences: Quo Vadis?" In: *Nat Methods* 19.9 (2022), pp. 1020–1025. ISSN: 1548-7091, 1548-7105. DOI: 10.1038/s41592-022-01602-3.

[7] Mad City Labs. *TIRF Lock™ | Keeps the Sample in the Focal Plane and Maintains TIRF Signal*. http://www.madcitylabs.com/tirf-lock.html. 2022.

[8] ASI Imaging. *CRISP Autofocus System | ASI*. https://www.asiimaging.com/products/focus-control-and-stabilization/crisp-autofocus-system/. 2015.

[9] Karl Bellve et al. "Design and Implementation of 3D Focus Stabilization for Fluorescence Microscopy". In: *Biophysical Journal* 106.2 (2014), 606a.

[10] Daniel Schröder et al. "Cost-Efficient Open Source Laser Engine for Microscopy". In: *Biomed. Opt. Express* 11.2 (2020), p. 609. ISSN: 2156-7085, 2156-7085. DOI: 10.1364/BOE.380815.

[11] Jeff Y.L. Lam et al. "An Economic, Square-Shaped Flat-Field Illumination Module for TIRF-based Super-Resolution Microscopy". In: *Biophysical Reports* 2.1 (2022), p. 100044. ISSN: 26670747. DOI: 10.1016/j.bpr.2022.100044.

[12] Andor. *Microscope Light Source | Integrated Laser Engine | ILE | Andor - Andor*. https://andor.oxinst.com/p components/integrated-laser-engine. 2022.

[13] John Philippi and Johannes Hohlbein. *SMILE: Single Molecule Imaging Laser Engine*. https://hohlbeinlab.gi 2022.

[14] Mohammed Mahamdeh and Erik Schäffer. "Optical Tweezers with Millikelvin Precision of Temperature-Controlled Objectives and Base-Pair Resolution". In: *Opt. Express* 17.19 (2009), p. 17190. ISSN: 1094-4087. DOI: 10.1364/OE.17.017190.

[15] Andy Maloney, Lawrence J. Herskowitz, and Steven J. Koch. "Effects of Surface Passivation on Gliding Motility Assays". In: *PLOS ONE* 6.6 (2011), e19522. ISSN: 1932-6203. DOI: 10.1371/journal.pone.0019522.

[16] Khalid A. Ibrahim, Dora Mahecic, and Suliana Manley. "Characterization of Flat-Fielding Systems for Quantitative Microscopy". In: *Opt. Express* 28.15 (2020), p. 22036. ISSN: 1094-4087. DOI: 10.1364/OE.395900.

[17] Ian Khaw et al. "Flat-Field Illumination for Quantitative Fluorescence Imaging". In: (2018), p. 13.

[18] Florian Stehr et al. "Flat-Top TIRF Illumination Boosts DNA-PAINT Imaging and Quantification". In: *Nat Commun* 10.1 (2019), p. 1268. ISSN: 2041-1723. DOI: 10.1038/s41467-019-09064-6.

[19] Paula Montero Llopis et al. "Best Practices and Tools for Reporting Reproducible Fluorescence Microscopy Methods". In: *Nat Methods* 18.12 (2021), pp. 1463–1476. ISSN: 1548-7091, 1548-7105. DOI: 10.1038/s41592-021-01156-w.

[20] Bioptechs. *Objective Heater – Bioptechs*. https://bioptechs.com/product/objective-heater/. 2022.

[21] Philip R. Nicovich et al. "NicoLase—An Open-Source Diode Laser Combiner, Fiber Launch, and Sequencing Controller for Fluorescence Microscopy". In: *PLOS ONE* 12.3 (2017), e0173879. ISSN: 1932-6203. DOI: 10.1371/journal.pone.0173879.

[22] CAIRN Research. *Triggerscope 4 | Core And Analysis | Cairn Research Ltd*. https://www.cairn-research.co.uk/product/triggerscope-4/. 2022.

[23] Teledyne. *OptoSplit III | Teledyne Photometrics*. https://www.photometrics.com/products/imaging-splitters/optosplit-iii. 2022.

[24] Benedict Diederich et al. "CAD We Share? Publishing Reproducible Microscope Hardware". In: *Nat Methods* 19.9 (2022), pp. 1026–1030. ISSN: 1548-7105. DOI: 10.1038/s41592-022-01484-5.

[25] Sara Abrahamsson et al. "MultiFocus Polarization Microscope (MF-PolScope) for 3D Polarization Imaging of up to 25 Focal Planes Simultaneously". In: *Opt. Express* 23.6 (2015), p. 7734. ISSN: 1094-4087. DOI: 10.1364/OE.23.007734.

[26] Rainer Heintzmann. "Practical Guide to Optical Alignment". In: *Fluorescence Microscopy*. John Wiley & Sons, Ltd, 2017. Chap. B, pp. 463–471. ISBN: 978-3-527-68773-2. DOI: 10.1002/9783527687732.app2.

[27] Arthur Edelstein et al. "Computer Control of Microscopes Using µManager". In: *Current Protocols in Molecular Biology* 92.1 (2010). ISSN: 1934-3639, 1934-3647. DOI: 10.1002/0471142727.mb1420s92.

[28] A. L. Mattheyses, S. M. Simon, and J. Z. Rappoport. "Imaging with Total Internal Reflection Fluorescence Microscopy for the Cell Biologist". In: *Journal of Cell Science* 123.21 (2010), pp. 3621–3628. ISSN: 0021-9533, 1477-9137. DOI: 10.1242/jcs.056218.

[29] Junel Sotolongo Bellón et al. "Four-Color Single-Molecule Imaging with Engineered Tags Resolves the Molecular Architecture of Signaling Complexes in the Plasma Membrane". In: *Cell Reports Methods* 2.2 (2022), p. 100165. ISSN: 26672375. DOI: 10.1016/j.crmeth.2022.100165.

[30] Kaley A. McCluskey et al. "Global Correction of Optical Distortions in Multicolor Single-Molecule Microscopy Using Zernike Polynomial Gradients". In: *Opt. Express* 29.25 (2021), p. 42251. ISSN: 1094-4087. DOI: 10.1364/OE.445230.

[31] Simao Coelho et al. "3D Active Stabilization for Single-Molecule Imaging". In: *Nat Protoc* 16.1 (2021), pp. 497–515. ISSN: 1754-2189, 1750-2799. DOI: 10.1038/s41596-020-00426-9.

[32] Sang Hak Lee et al. "Using Fixed Fiduciary Markers for Stage Drift Correction". In: *Opt. Express* 20.11 (2012), p. 12177. ISSN: 1094-4087. DOI: 10.1364/OE.20.012177.

[33] Ryan McGorty, Daichi Kamiyama, and Bo Huang. "Active Microscope Stabilization in Three Dimensions Using Image Correlation". In: *Opt Nano* 2.1 (2013), p. 3. ISSN: 2192-2853. DOI: 10.1186/2192-2853-2-3.

[34] Yeoan Youn et al. "Thermal Nanoimprint Lithography for Drift Correction in Super-Resolution Fluorescence Microscopy". In: *Opt. Express* 26.2 (2018), p. 1670. ISSN: 1094-4087. DOI: 10.1364/OE.26.001670.

[35] Smaract. *Stick-Slip Drive Technology*. https://www.smaract.com/en/technology-introduction-and-options#position-sensors. 2022.

[36] ASI. *MS-2000 XYZ Automated Stage | ASI*. https://www.asiimaging.com/products/stages/xy-inverted-stages/ms-2000-xyz-automated-stage/. 2022.

[37] Carsen Stringer et al. “Cellpose: A Generalist Algorithm for Cellular Segmentation”. In: *Nat Methods* 18.1 (2021), pp. 100–106. ISSN: 1548-7091, 1548-7105. DOI: 10.1038/s41592-020-01018-x.

[38] Dmitry Ershov et al. “TrackMate 7: Integrating State-of-the-Art Segmentation Algorithms into Tracking Pipelines”. In: *Nat Methods* 19.7 (2022), pp. 829–832. ISSN: 1548-7091, 1548-7105. DOI: 10.1038/s41592-022-01507-1.

[39] E. N. Hogert, Jose J. Lunazzi, and Nestor G. Gaggioli. “Visual Speckle Technique for Alignment and Centering of a Translucent Rough Surface”. In: *Appl. Opt.* 28.4 (1989), p. 722. ISSN: 0003-6935, 1539-4522. DOI: 10.1364/AO.28.000722.

[40] Matthew T. Pandina. *Ghost-It! 1.04*. https://www.majorgeeks.com/files/details/ghost_it.html. 2022.

[41] Stephan Preibisch, Stephan Saalfeld, and Pavel Tomancak. “Globally Optimal Stitching of Tiled 3D Microscopic Image Acquisitions”. In: *Bioinformatics* 25.11 (2009), pp. 1463–1465. ISSN: 1367-4803. DOI: 10.1093/bioinformatics/btp184.

[42] Johannes Schindelin et al. “Fiji: An Open-Source Platform for Biological-Image Analysis”. In: *Nature Methods* 9.7 (2012), pp. 676–682. ISSN: 1548-7105. DOI: 10.1038/nmeth.2019.